Chemical Science

ROYAL SOCIETY OF CHEMISTRY

EDGE ARTICLE

View Article Online
View Journal | View Issue

Cite this: *Chem. Sci.*, 2023, **14**, 2353

All publication charges for this article have been paid for by the Royal Society of Chemistry

Received 23rd October 2022
Accepted 3rd January 2023

DOI: 10.1039/d2sc05858h

rsc.li/chemical-science

Saddle-shaped aza-nanographene with multiple odd-membered rings†

Maciej Krzeszewski,[a] Łukasz Dobrzycki,[b] Andrzej L. Sobolewski,*[c] Michał K. Cyrański*[b] and Daniel T. Gryko*[a]

A saddle-shaped aza-nanographene containing a central 1,4-dihydropyrrolo[3,2-*b*]pyrrole (DHPP) has been prepared *via* a rationally designed four-step synthetic pathway encompassing intramolecular direct arylation, the Scholl reaction, and finally photo-induced radical cyclization. The target non-alternant, nitrogen-embedded polycyclic aromatic hydrocarbon (PAH) incorporates two abutting pentagons between four adjacent heptagons forming unique 7–7–5–5–7–7 topology. Such a combination of odd-membered-ring defects entails a negative Gaussian curvature within its surface with a significant distortion from planarity (saddle height ≈ 4.3 Å). Its absorption and fluorescence maxima are located in the orange-red region, with weak emission originating from the intramolecular charge-transfer character of a low-energy absorption band. Cyclic voltammetry measurements revealed that this stable under ambient conditions aza-nanographene underwent three fully reversible oxidation steps (two one-electron followed by one two-electron) with an exceptionally low first oxidation potential of E_{ox1} = −0.38 V (*vs.* Fc/Fc$^+$).

Introduction

The discovery of curved carbon allotropes, *i.e.* fullerenes[1] and cylindrical carbon nanotubes[2] has resulted in a paradigm shift in the chemistry of polyarenes and has given rise to modern materials science. Aromatic compounds, which in the early days of organic chemistry were considered to have a tendency to be planar, can actually adopt various nonplanar molecular shapes.[3,4] The development of contemporary synthetic methods in combination with researchers' imagination and creativity has enabled the preparation of elusive, three-dimensional structures including circulenes,[5–9] cycloparaphenylenes (CPPs),[10–13] carbon nanobelts (CNBs),[14–18] large phenine frameworks[19,20] and impressive, all-benzene interlocked catenanes and trefoil knots.[21] Moreover, embedding non-hexagonal rings in a graphenic lattice causes warping of the π-system, due to geometric mismatch of adjacent rings. The presence of a five-membered ring introduces a positive Gaussian curvature as in the case of the smallest curved cutouts of C_{60}, *i.e.* corannulene,[22–26] and sumanene[27,28] and their π-extended analogs,[29–32] while the incorporation of rings larger than hexagons *e.g.* heptagons[33] or octagons[34] leads to a negative curvature and a saddle-shaped geometry (Fig. 1a).[30,35–39] The chemistry of distorted molecular nanocarbons continues to evolve, not only as a consequence of curiosity or aesthetic appeal, but also due to their concrete contribution to understanding the inherent nature of aromaticity,[40–44] by delivering experimental verification for the distribution of electrons in their π-extended scaffolds.[45,46]

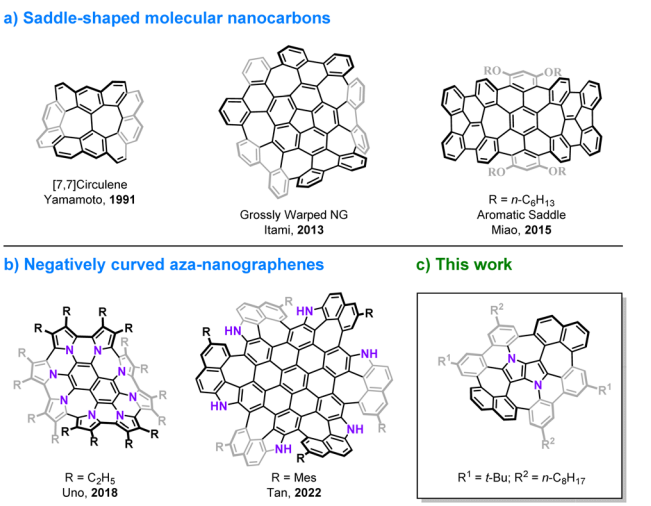

Fig. 1 Representative examples of negatively curved polyarenes containing multiple odd-membered rings.

[a]*Institute of Organic Chemistry, Polish Academy of Sciences, Kasprzaka 44-52, 01-224 Warsaw, Poland. E-mail: dtgryko@icho.edu.pl*

[b]*Faculty of Chemistry, University of Warsaw, Żwirki i Wigury 101, 02-089 Warsaw, Poland. E-mail: mkc@chem.uw.edu.pl*

[c]*Institute of Physics, Polish Academy of Sciences, Al. Lotników 32/46, 02-668 Warsaw, Poland. E-mail: sobola@ifpan.edu.pl*

† Electronic supplementary information (ESI) available: Details of the synthesis and spectroscopic characterization of new compounds, crystallographic and electrochemical data. CCDC 2210403. For ESI and crystallographic data in CIF or other electronic format see DOI: https://doi.org/10.1039/d2sc05858h

Furthermore, history has shown that the emergence of various carbon allotropes has indeed led to the discovery of previously unforeseen and unpredicted functions and applications.[47,48] Doping heteroatoms into a carbonaceous backbone of the π-systems is an elegant and efficient method of tuning their basic physicochemical and electronic characteristics.[49,50] In particular, interest in nitrogen-embedded, nonplanar polyarenes has gained significant momentum recently, resulting in the construction of some intriguing, mainly positively curved molecules.[51–56] Examples of negatively curved aza-nanographenes, however, remain rather scarce (Fig. 1b).[57–60] Here, we present the synthesis and properties of a saddle-shaped polyarene containing the most electron-rich small aromatic molecule, 1,4-dihydropyrrolo[3,2-*b*]pyrrole.[61] This 16-ring nitrogen-containing molecular nanocarbon comprises two central pentagons confined between four adjacent heptagons, a lattice defect, which to the best of our knowledge, has not yet been identified in graphene.[62–64]

Results and discussion

Design and synthesis

Recently, we reported the on-surface,[65] followed by an in-solution[66] syntheses of an aza-buckybowl composed of a 1,4-dihydropyrrolo[3,2-*b*]pyrrole (DHPP) core encircled by six benzene rings bonded with each other, possessing the inverse Stone–Thrower–Wales (7–5–5–7) defect. In the latter endeavor, the implemented synthetic pathway encompassed DHPP formation, the Scholl reaction,[67–70] and subsequent sequential intramolecular direct arylation.[71] The success of the applied synthetic strategy leading to a series of consecutive couplings of peripheral rings around the central DHPP core prompted us to design and prepare a saddle-shaped DHPP-based nanographene. We envisaged that a seemingly small modification in the structure, *i.e.*, replacing two hexagons with two heptagons next to the central unit (Fig. 2) realized by an imaginary 'insertion' of additional benzene rings (naphthalene *vs.* benzene) would entail a drastic change in the molecular geometry and thus in the overall physicochemical features.

We began with designing a suitable DHPP which would be a platform for further intramolecular transformations. Our analysis resulted in a tetra-aryl pyrrolo[3,2-*b*]pyrrole (TAPP) substituted with two 2-(naphthalen-2-yl)phenyl groups on the pyrrolic nitrogen atoms and two phenyl residues at positions 2 and 5 of the pyrrolo[3,2-*b*]pyrrole unit, both carrying a bromine and a chlorine atom at their *ortho* positions. Finally, to ensure sufficient solubility of the final compound and its parent precursors in common organic solvents, we decided to introduce two *tert*-butyl groups and two *n*-octyl chains on the periphery.

Consequently, suitable starting materials were prepared, that is, 2-bromo-4-(*tert*-butyl)-6-chlorobenzaldehyde (**1**) and 2-(naphthalen-2-yl)-4-octylaniline (**2**) (see the ESI† for details). The one-pot multicomponent condensation, catalyzed by iron(III) perchlorate,[72] between **1**, **2** and butane-2,3-dione (**3**) gave TAPP **4** in 49% yield (Scheme 1). Compound **4** was then subjected to selective intramolecular direct arylation through exclusive double C–Br activation, while the two C–Cl bonds remained intact. The reaction was carried out with $Pd(OAc)_2$, Cs_2CO_3 and PPh_3 in toluene at 120 °C for 4 h, giving compound **5** in excellent yield (91%). Then, this product was subjected to the double Scholl reaction mediated by iron(III) triflate. Importantly, as we have already demonstrated, the specific order of consecutive steps is crucial to avoid the unwanted 1,2-aryl shift triggered by the oxidative aromatic coupling.[73,74] Also, as previously reported, $FeCl_3$ proved to be the most efficient oxidizing agent with respect to interactions with DHPPs; however, in this particular case, side products were formed. As shown before, the excessive amount of $FeCl_3$ could lead to undesired chlorination of the PP core.[66] Therefore, we used iron(III) triflate instead to exclude the possibility of any uncontrolled chlorination processes.[75] The reaction was carried out in a dichloroethane/nitromethane mixture at 80 °C for 6 h. The desired compound **6** containing two newly formed seven-membered rings was isolated with a yield of 24%, which is only slightly lower (24% *vs.* 29%) than the yield of the analogous Scholl reaction carried out on the synthesis of the aza-buckybowl reported earlier.[66] It is worth mentioning that this reaction is highly regioselective, and double oxidation takes place predominantly at the α-positions of both naphthalene subunits, which was unequivocally confirmed by X-ray diffraction (Scheme 1, inset). Then, the rationally designed compound **6** was subjected to the final double C–Cl bond activation. The reaction was carried out with $Pd(OAc)_2$ and HP*t*-Bu_2MeBF_4 in a mixture of DBU/DMA in a pressure tube at 180 °C for 24 h. However, it turned out that the desired coupling took place only on one side of the molecule, whereas dehalogenation occurred on the other side, giving a saddle–helicene hybrid **7** isolated in 52% yield. Therefore, we resorted to a different strategy, namely photo-induced radical cyclization.[60] To our delight, subjecting **6** to a reaction with potassium *tert*-butoxide in DMSO irradiated with 455 nm blue LEDs at ambient temperature for 20 h gave the desired saddle-shaped nanographene **8** with a yield of 75%.

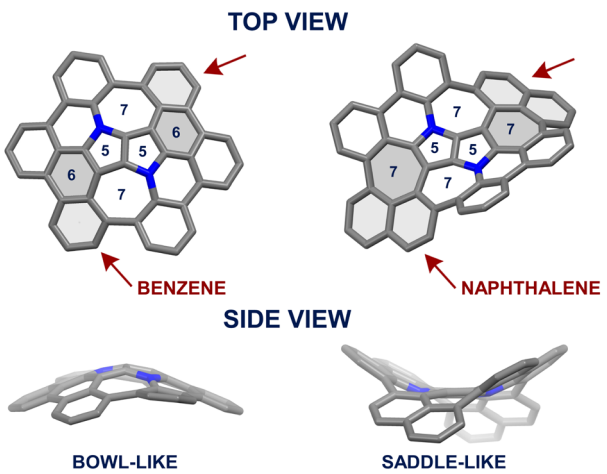

Fig. 2 Left-hand side: crystal structure (CCDC 2064960†)[66] of bowl-shaped DHPP-based nanographene. Right-hand side: the computed model of its π-extended counterpart adopting a saddle-shaped geometry.

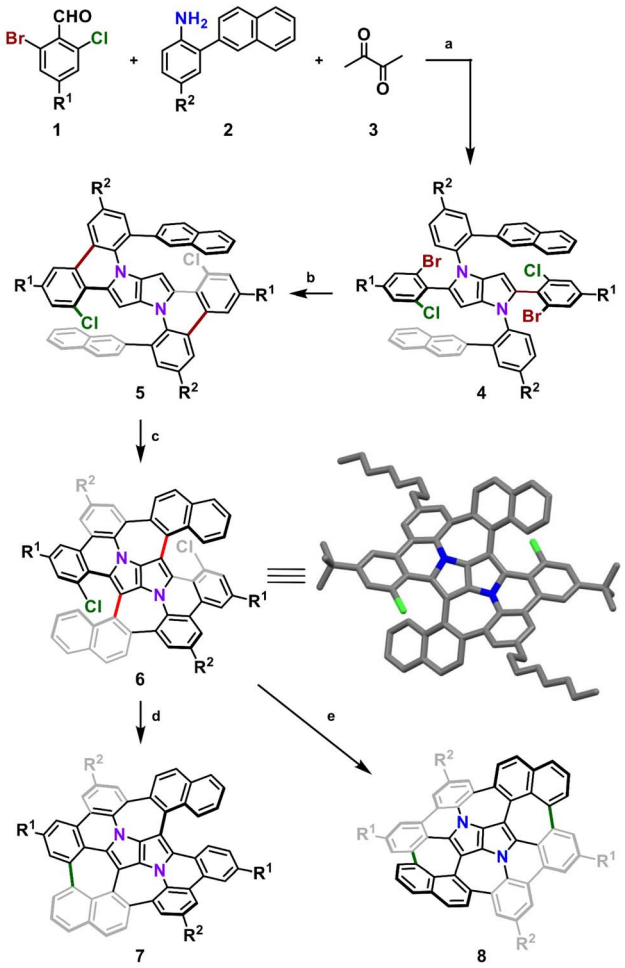

Scheme 1 Synthetic route to molecular saddle **8**. Reagents and conditions: (a) $Fe(ClO_4)_3 \cdot xH_2O$ (6 mol%), AcOH/toluene, 50 °C, 16 h, 49%; (b) $Pd(OAc)_2$ (20 mol%), Cs_2CO_3 (2.4 equiv.), PPh_3 (48 mol%), toluene, 120 °C, 4 h, 91%; (c) $Fe(OTf)_3$ (6.0 equiv.), DCE/$MeNO_2$, 80 °C, 6 h, 24%; (d) $Pd(OAc)_2$ (2.0 equiv.), HP*t*-Bu_2MeBF_4 (6.0 equiv.), DBU/DMA, 180 °C, 24 h, 52%; (e) *t*-BuOK (10.0 equiv.), DMSO, blue LEDs, rt, 20 h, 75%. DMA – dimethylacetamide, DCE – 1,2-dichloroethane; inset: X-ray crystal structure of **6**. $R^1 = t$-Bu, $R^2 = n$-C_8H_{17}.

Its structure was confirmed through nuclear magnetic resonance (NMR) spectroscopy, and high-resolution mass spectrometry (HRMS). Its superb solubility allowed for NMR measurements in cyclohexane-d_{12}. The variable temperature ^{1}H NMR spectrum of nanographene **8** measured in cyclohexane-d_{12} at 10–60 °C (Fig. 3) reveals the dynamic behavior of the molecule in solution and rapid equilibration of naphthalene protons on the perimeter (Fig. 3). Further 2D-NMR studies allowed each signal to be assigned to the respective proton (see the ESI† for details).

X-ray crystallography analysis

In spite of many attempts it was not possible to crystallize the final product **8**, only an amorphous solid was obtained instead. However, during slow evaporation of THF/MeOH/acetone solution X-ray quality crystals of the intermediate compound

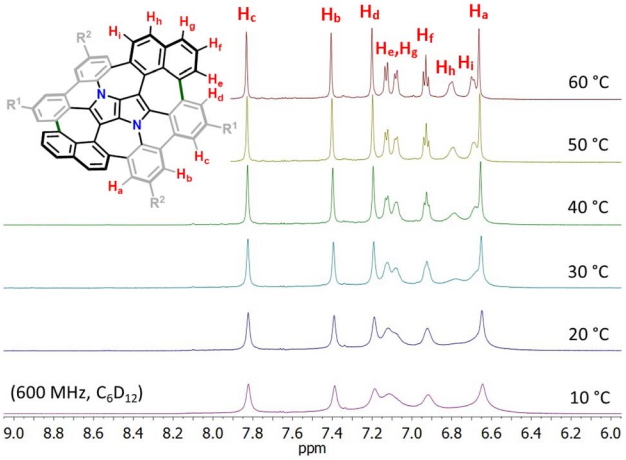

Fig. 3 Variable temperature ^{1}H-NMR spectrum of the molecular N-doped saddle **8** in the aromatic region (from 6.0 to 9.0 ppm) recorded in cyclohexane-d_{12} (600 MHz, 10–60 °C).

6 were obtained confirming its anticipated structure. All the details concerning the crystal data and the structure refinement are located in Table S1 of the ESI.† The crystal lattice contains two centrosymmetric conformers of **6** with slightly different geometry. Hence, the symmetry of the molecule from the X-ray studies fully agrees with the NMR data. The structure is severely disordered especially in the *n*-octyl chains. The overlay of the two molecules with adjacent five-membered rings atoms fitted is presented in Fig. 4. As it can be seen the core of the molecules fits almost ideally, even seven-membered rings are distorted to the same extent. Whereas the biggest geometry difference

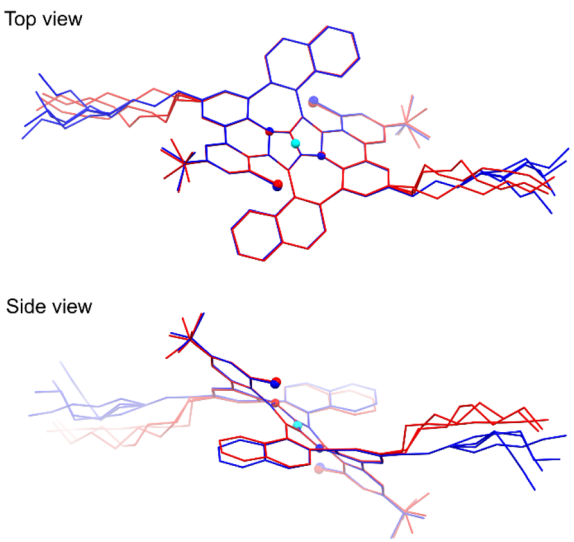

Fig. 4 Top and side views of the overlay of two differently colored molecules form the crystal structure of **6** (CCDC 2210403†). The cyan sphere represents the center of symmetry; smaller and bigger globes denote the N and Cl atoms, respectively. Overlay was performed for all eight atoms of two adjacent five-membered rings. The THF molecule and all H atoms have been omitted for clarity.

occurs in the alkyl chains, the naphthalene moieties deviate as well.

Theoretical investigation of conformational flexibility

Quantum chemical calculations were performed for the aza-nanographene **8** structure with the *tert*-butyl groups and octyl-chains replaced by hydrogen atoms (**8H**). The equilibrium geometries of the possible conformers of **8H** and the saddle-points between them in the closed-shell ground state (S_0) were determined with the MP2 method. Local minima and saddle-points were verified by computation of the Hessian of the DFT-optimized structures (see the ESI† for details). The dense accumulation of non-hexagonal rings around the central point of **8H** leads to its double-concave molecular structure (Fig. 5). The central DHPP core is nearly planar, while the peripheral phenanthridine and naphthalene components are heavily twisted out of plane to give a saddle height of 4.3 Å (Fig. 5b). These moieties arrange themselves in such a way that both naphthalene subunits are facing downwards and simultaneously both phenanthridine subunits are facing upwards (or conversely, in the case of its enantiomer) (Fig. 5a). The racemization mechanism of (*M*,*P*,*M*,*P*)-**8H** to (*P*,*M*,*P*,*M*)-**8H** follows a complex quintuple-well potential model through two transition states TS1 and TS2 and the *meso* form (*M*,*M*,*P*,*P*)-**8H**. The calculated energy barrier of 19.6 kcal mol^{-1} is very similar to that of Itami's grossly warped nanographene (theoretical value: 18.9 kcal mol^{-1}).[30] Although the racemization energy barrier is markedly higher than that of the DHPP-based buckybowl (theoretical value: 5.4 kcal mol^{-1}),[66] it is still not high enough to ensure conformational stability at ambient temperature, which is supported by the variable temperature ^{1}H NMR experiments (*vide supra*). The overall potential-energy (PE) landscape of the racemization process of **8H** is shown in Fig. 5d.

Photophysical and electrochemical properties

In order to unravel the impact of the molecular geometry and the consecutive extensions of the π-system on the overall photophysical characteristics, we measured the UV-vis absorption and fluorescence spectra of compounds **4–8**. The results are shown in Table 1 and Fig. 6. The tetraaryl-substituted DHPP **4** shows a main absorption band comprising two peaks located in

Table 1 Spectroscopic and electrochemical properties of compounds **4–8** [a]

Cmpd.	λ_{abs} [nm]	$\varepsilon \times 10^3$ [M^{-1} cm^{-1}]	λ_{em} [nm]	Φ_{fl} [b]	E_{ox1} [1/2c] [V]	E_{HOMO} [eV]
4	346	14	—	—	0.35	−5.15
5	410	20	534	0.14	0.05	−4.85
6	432	22	601	0.023	0.18	−4.98
7	461	16	622	0.034	−0.12	−4.68
8	468	17	623	0.038	−0.38	−4.42

[a] Measured in CH_2Cl_2. [b] Determined with coumarin 153 in EtOH as a standard. [c] Cyclic voltammograms were measured in a deoxygenated solution of 0.1 M tetrabutylammonium perchlorate in anhydrous CH_2Cl_2, with a glassy-carbon working electrode, a Ag/AgCl/$NaCl_{sat}$ reference electrode, and a platinum-foil auxiliary electrode (scan rate ν = 100 mV s^{-1}, Ar, rt). Oxidation potentials are given relative to Fc/Fc$^+$.

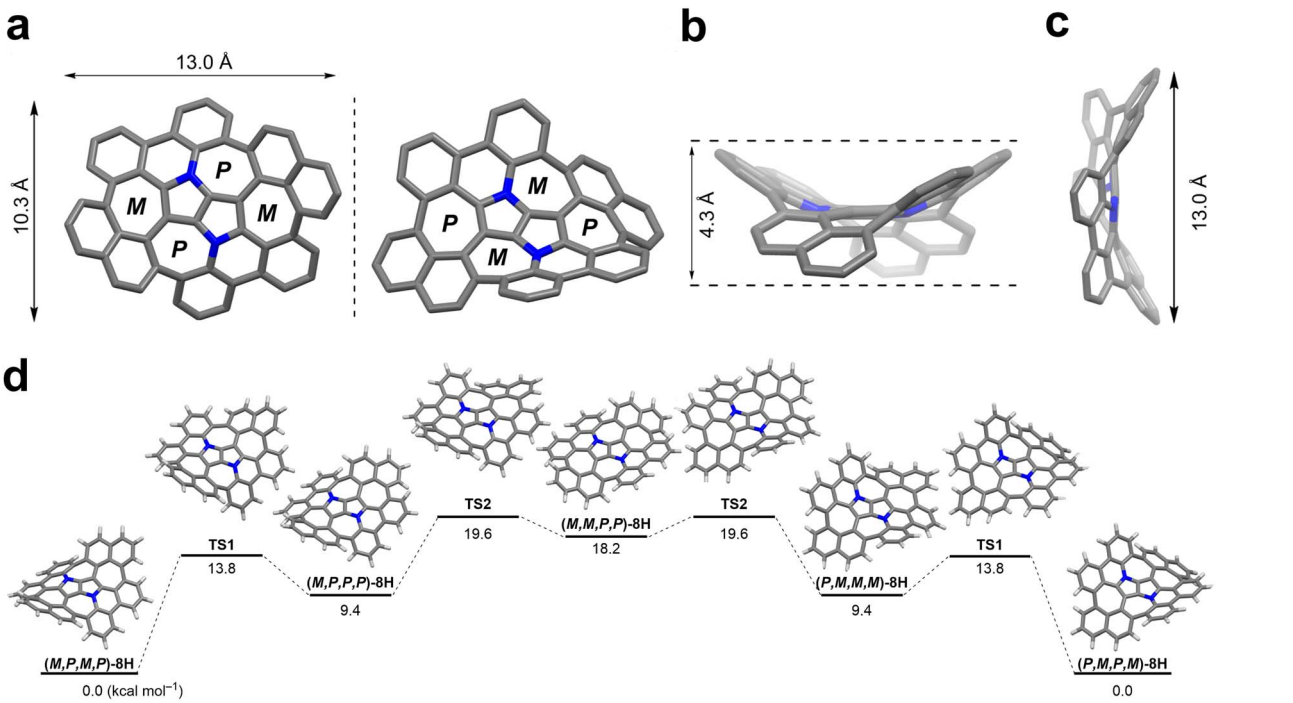

Fig. 5 Images showing the warped structure of the truncated molecular saddle **8H**. (a) Top view of the **8H** enantiomer pair. (b) Side view along the *a* axis. (c) Side view along the *b* axis. (d) The potential energy landscape of **8H**. All geometries were optimized at the MP2/cc-pVDZ level of theory (zero-point energy corrected).

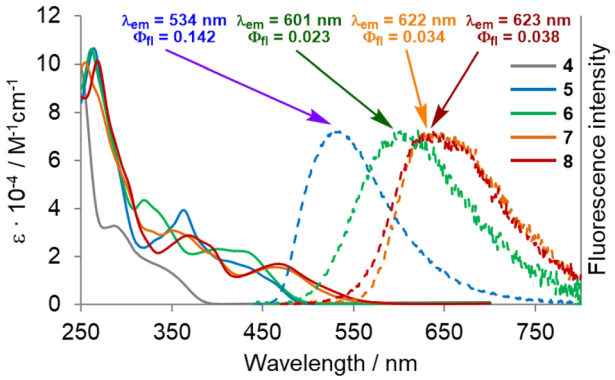

Fig. 6 UV-vis absorption spectra (solid lines) and fluorescence spectra (dashed lines) of dyes **4**–**8** measured in dichloromethane.

the ultraviolet region of the spectrum at $\lambda_{abs} = 285$ and 334 nm with molar extinction coefficients (ε) reaching 33 000 M^{-1} cm^{-1} and 16 000 M^{-1} cm^{-1}, respectively. Dye **5** obtained from **4** through intramolecular direct arylation possesses a higher degree of conjugation, which is clearly manifested in its optical features. A large bathochromic shift in absorption is observed, accompanied by a hyperchromic shift. Moreover, unlike **4**, compound **5** exhibits an emission. In its absorption spectrum, there are two broad bands, the first located between 320 and 400 nm and the second between 400 and 450 nm with a shoulder extending to *ca.* 480 nm. Higher-energy transitions show a peak located at $\lambda_{abs} = 362$ nm with $\varepsilon = 39\,000$ M^{-1} cm^{-1}. Lower-energy transitions exhibit faint maxima at *ca.* $\lambda_{abs} = 410$ with shoulders at 430 and 460 nm (ε = 18 000, 16 000 and 10 000 M^{-1} cm^{-1}). Dye **5** is a weak green light emitter ($\lambda_{em} = 534$ nm) with a fluorescence quantum yield (Φ_{fl}) of 0.14. The fluorescence maximum of **6**, possessing two seven-membered rings, is strongly bathochromically shifted (67 nm) with respect to **5** ($\lambda_{em} = 601$ *vs.* 534 nm) with an accompanying evident decrease in emission intensity to $\Phi_{fl} = 0.023$. The unusually high Stokes' shift value determined for **6**, namely 6500 cm^{-1} (169 nm), stems from the profound differences in its S_1 excited state and S_0 ground state geometries.

In both cases of π-extension, leading to compounds **7** and **8**, a red-shift of the absorption and emission spectra can be observed. The final saddle-shaped aza-nanographene **8** exhibits three prominent bands in the absorption spectrum. The first band is located between 280 and 330 nm with a distinctive shoulder at 300 nm with $\varepsilon = 52\,000$ M^{-1} cm^{-1}. The second band corresponding to lower-energy transitions, found between 330 and 420 nm, shows a peak at λ_{abs} = 367 nm (ε = 29 000 M^{-1} cm^{-1}) with a shoulder at 390 nm (ε = 25 000 M^{-1} cm^{-1}). Finally the third band corresponds to the longest wavelength absorption at 468 nm, $\varepsilon = 17\,000$ M^{-1} cm^{-1} tailing up to 580 nm. The maximum absorption is red-shifted by 7 nm compared to **7**. Interestingly, both compounds **7** and **8** have nearly identical emission maxima in the orange/red region of the spectrum with $\lambda_{em} = 622$ and 623 nm, and exhibit similar fluorescence quantum yields of Φ_{fl} = 0.034 and 0.038, respectively. Unlike the DHPP-buckybowl,[66] molecular saddle **8** does not show any dependence of the emission features on solvent polarity (see the ESI† for details).

A direct comparison of the photophysics of dye **8** with the previously reported aza-buckybowl[66] reveals that they behave in analogous manner. In both cases absorption peaks at approx. 470 nm with long tail reaching beyond 550 nm. Both the aza-buckybowl and **8** possess a broad, weak red emission. A more pronounced deformation of the molecule **8** is reflected by a small bathochromic shift of the emission maximum by *ca.* 8 nm compared to the respective buckybowl.

To further elucidate the nature of electronic transitions, the absorption spectrum of the lowest-energy conformer (*M*,*P*,*M*,*P*)-**8H** was computed with the aid of two different theoretical methods: TD-DFT and ADC(2). The resulting spectrum is shown in Fig. S13 of the ESI.† Apart from the expected energy shift, both computed spectra are consistent with each other and are in good agreement with the low-energy part of the observed absorption spectrum of **8**.

The photophysical parameters of the lowest excited states of **8H** computed with the aid of the ADC(2)/cc-pVDZ *ab initio* method are summarized in Table S3 of the ESI.† On inspection of the results it can be noticed that the series of excited singlet states that comprise the low-energy part of the absorption spectrum involve electronic excitations from the two highest occupied molecular orbitals (HOMO−2 and HOMO) in the C_2 symmetry point group of the (*M*,*P*,*M*,*P*)-**8H** conformer. Both HOMOs are localized largely on the DHPP core. Optical excitation of the system expels an electron from the central core into the (naphthalene and benzene) molecular edges (Fig. 7).

Geometry optimization of the two lowest excited singlet states ($^1A(S_1)$ and $^1B(S_2)$) with the aid of the ADC(2) method resulted in the determination of their adiabatic energy and energy of the vertical fluorescence expected from these states (Fig. 8). Additionally, the natural transition orbitals (NTOs)[76] of the hole and the electron created by electronic excitation of these states were determined. These data are shown in Fig. S14 of the ESI.† From this it can be seen that both states are stabilized by a similar energy loss due to geometry optimization, and the state of the A symmetry is by about 0.22 eV (5.1 kcal mol^{-1}) more stable than the state of the B symmetry, both 'vertically' (Table S3†) and adiabatically (Fig. S14†). The singlet state of the B symmetry lies above the ^1A even at the optimized geometry of the former state. We therefore conclude that the latter state represents the lowest (emitting) singlet state (S_1) of the **8H** (and **8**) compound, although its oscillator strength for emission is one order of magnitude smaller than for emission from the ^1B state (Fig. S14†). The NTOs inspection of the two excited states indicates that the fluorescence from these states is approximately perpendicularly polarized to each other.

Finally, the well-known, electron-rich nature of 1,4-dihydropyrrolo[3,2-*b*]pyrroles renders them potent candidates for application in the field of organic optoelectronics. Therefore, voltammetric experiments were performed to investigate the electrochemical properties of all synthesized DHPP-based compounds **4**–**8**. Cyclic voltammetry measurements revealed that all obtained DHPPs are easily oxidizable with the obvious trend that as the degree of conjugation is increased, the lower

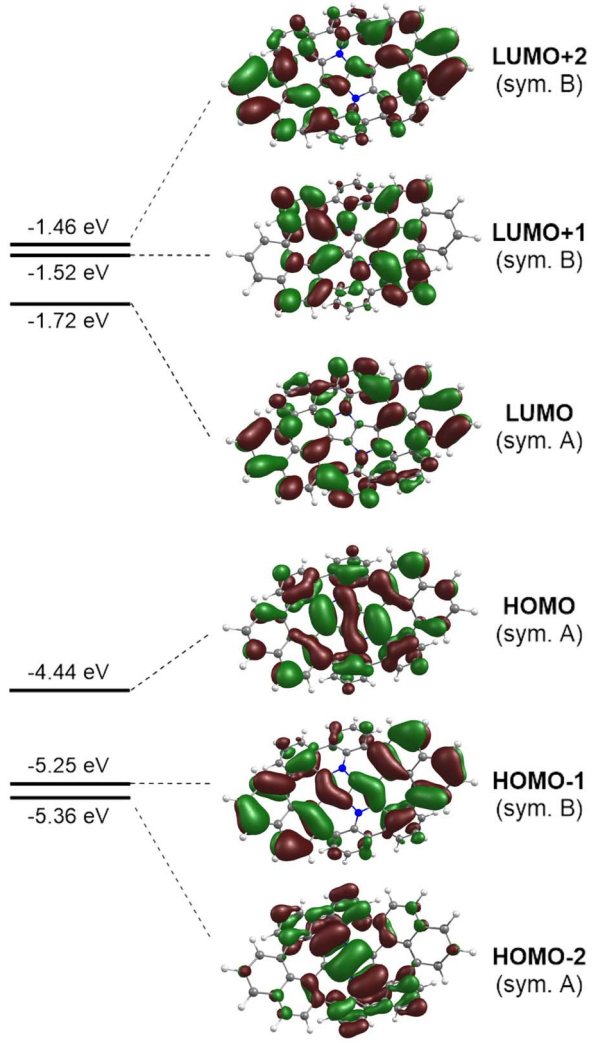

Fig. 7 Selected Kohn–Sham molecular orbitals of the truncated molecular saddle **8H** and their energy levels calculated with the aid of DFT at the B3LYP/cc-pVDZ level of theory. An isovalue of 0.02 was used for the depiction of each MO, the view corresponds to the top face of the molecule.

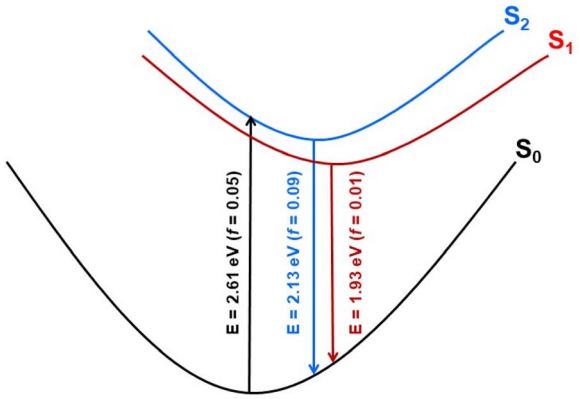

Fig. 8 Schematic potential energy profiles of the lowest excited states of **8H** constructed on the basis of theoretical results. Vertical arrows illustrate vertical absorption from the ground state (black) and fluorescence (blue and red) from the lowest excited singlet states with values of transition energy (*E*) and oscillator strength (*f*) computed at the ADC(2)/cc-pVDZ theoretical level.

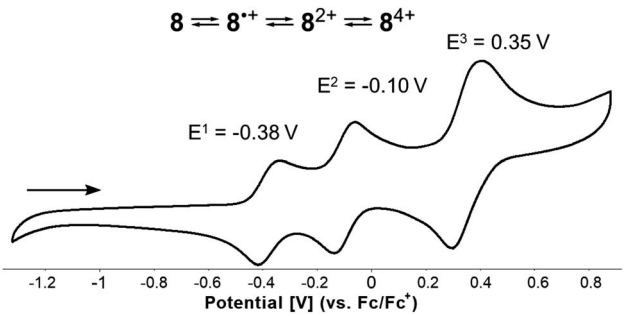

Fig. 9 Cyclic voltammogram of the N-doped molecular saddle **8**.

the first oxidation potential (Tables 1 and S2†). The parent TAPP **4**, underwent two one-electron oxidation steps, the first being reversible, followed by an irreversible process. Concurrently compounds **5–7** underwent two one-electron reversible oxidation steps (see the ESI†). Intriguingly, target molecular saddle **8** underwent as many as three fully reversible oxidation steps. The first two were one-electron processes, whereas the third was two-electron process. The half-wave potentials measured for **8** referenced to the ferrocene/ferrocenium ion couple were $E_{ox1} = -0.38$ V, $E_{ox2} = -0.10$ V, and $E_{ox3} = +0.35$ V (Fig. 9). HOMO energy levels (E_{HOMO}) were estimated from the first oxidation potentials (Table 1). The calculated energy of the HOMO level of **8H** ($E_{HOMO} = -4.44$ eV, Fig. 7) was in excellent agreement with the experimental data for **8** *i.e.*, $E_{HOMO} = -4.42$ eV. Thus, HOMO of dye **8** is located *ca.* 0.3 eV above HOMO of previously described buckybowl ($E_{HOMO} = -4.71$ eV).[66] The exceptionally low value of the first oxidation potential of **8**, nearly as low as the potential measured for the core-expanded azacoronene that has up to eight nitrogen atoms ($E_{ox1} = -0.52$ V)[57] indicates its remarkable tendency to oxidize. To date, this is a record-breaking oxidation potential value in the chemistry of dihydropyrrolopyrroles.[77]

Conclusions

By employing a rationally designed synthetic strategy, we have demonstrated the successful solution phase synthesis of a saddle-shaped aza-nanographene containing a pyrrolopyrrole core. This 16-ring nitrogen-doped, highly twisted framework was easily and efficiently formed in four steps with an overall yield of 8%. Our approach undoubtedly shows that the constant growth of the synthetic toolbox allows scientists to fine-tune the structure and properties of previously unimaginable organic materials. This heavily distorted π-system provides valuable information regarding the impact of closely concentrated odd-membered-ring defects on the overall physicochemical properties of the otherwise planar graphenic sheet. To the best of our knowledge this is the first nanographene displaying a unique 7–7–5–5–7–7 topology. Furthermore, it is the first example of a π-extended 1,4-dihydropyrrolo[3,2-*b*]pyrrole that exhibits three

fully reversible oxidation steps, with a record low for its first oxidation potential value. We have proven that replacing the previously described 7–5–5–7 ring system with 7–7–5–5–7–7 one leads to three dramatic changes: (1) the new aza-nanographene is markedly (0.3 eV) easier to oxidize; (2) distortion from planarity doubles (4.3 Å *vs.* 2.1 Å) and (3) negative curvature replaces positive curvature. The warped double-concave structure holds potential for supramolecular research and its use in the construction of future outstanding nitrogen-enriched nanocarbon materials is envisioned.

Data availability

The data supporting this article have been uploaded as part of the ESI.†

Author contributions

M. K. conceived the idea and wrote the manuscript. M. K. performed all synthetic experiments. Ł. D. performed crystallographic studies and M. K. C. supervised them. A. L. S. performed computational studies, analyzed data, wrote and reviewed the manuscript. D. T. G. supervised the project, performed formal analysis, wrote and reviewed the manuscript. All the authors discussed the results and commented on the manuscript. All authors have given approval to the final version of the manuscript.

Conflicts of interest

There are no conflicts to declare.

Acknowledgements

The work was financially supported by the Polish National Science Centre, Poland (OPUS 2020/37/B/ST4/00017), the Foundation for Polish Science (TEAM POIR.04.04.00-00-3CF4/16-00 and START scholarship no. 039.2017 to M. K.). M. K. is a recipient of a scholarship awarded by the Polish Ministry of Education and Science to outstanding young scientists. The authors thank Dr David C. Young for proofreading the manuscript.

Notes and references

1 H. W. Kroto, J. R. Heath, S. C. O'Brien, R. F. Curl and R. E. Smalley, *Nature*, 1985, **318**, 162–163.
2 S. Iijima, *Nature*, 1991, **354**, 56–58.
3 M. A. Majewski and M. Stępień, *Angew. Chem.*, 2019, **131**, 90–122.
4 Y. Segawa, D. R. Levine and K. Itami, *Acc. Chem. Res.*, 2019, **52**, 2760–2767.
5 (*a*) S. K. Pedersen, K. Eriksen, H. Ågren, B. F. Minaev, N. N. Karaush-Karmazin, O. Hammerich, G. V. Baryshnikov and M. Pittelkow, *J. Am. Chem. Soc.*, 2020, **33**, 14058–14063; (*b*) K. Yamamoto, T. Harada, M. Nakazaki, T. Naka, Y. Kai, S. Harada and N. Kasai, *J. Am. Chem. Soc.*, 1983, **105**, 7171–7172.
6 K. Yamamoto, Y. Saitho, D. Iwaki and T. Ooka, *Angew. Chem., Int. Ed.*, 1991, **30**, 1173–1174.
7 C. N. Feng, M. Y. Kuo and Y. T. Wu, *Angew. Chem., Int. Ed.*, 2013, **52**, 7791–7794.
8 Y. Sakamoto and T. Suzuki, *J. Am. Chem. Soc.*, 2013, **135**, 14074–14077.
9 M. Krzeszewski, H. Ito and K. Itami, *J. Am. Chem. Soc.*, 2022, **144**, 862–871.
10 R. Jasti, J. Bhattacharjee, J. B. Neaton and C. R. Bertozzi, *J. Am. Chem. Soc.*, 2008, **130**, 17646–17647.
11 H. Takaba, H. Omachi, Y. Yamamoto, J. Bouffard and K. Itami, *Angew. Chem., Int. Ed.*, 2009, **48**, 6112–6116.
12 S. Yamago, Y. Watanabe and T. Iwamoto, *Angew. Chem., Int. Ed.*, 2010, **49**, 757–759.
13 F. E. Golling, S. Osella, M. Quernheim, M. Wagner, D. Beljonne and K. Müllen, *Chem. Sci.*, 2015, **6**, 7072–7078.
14 G. Povie, Y. Segawa, T. Nishihara, Y. Miyauchi and K. Itami, *Science*, 2017, **356**, 172–175.
15 G. Povie, Y. Segawa, T. Nishihara, Y. Miyauchi and K. Itami, *J. Am. Chem. Soc.*, 2018, **140**, 10054–10059.
16 K. Y. Cheung, S. Gui, C. Deng, H. Liang, Z. Xia, Z. Liu, L. Chi and Q. Miao, *Chem*, 2019, **5**, 838–847.
17 K. Y. Cheung, K. Watanabe, Y. Segawa and K. Itami, *Nat. Chem.*, 2021, **13**, 255–259.
18 Y. Segawa, T. Watanabe, K. Yamanoue, M. Kuwayama, K. Watanabe, J. Pirillo, Y. Hijikata and K. Itami, *Nat. Synth.*, 2022, **1**, 535–541.
19 K. Ikemoto, J. Lin, R. Kobayashi, S. Sato and H. Isobe, *Angew. Chem., Int. Ed.*, 2018, **57**, 8555–8559.
20 K. Ikemoto, M. Akiyoshi, T. Mio, K. Nishioka, S. Sato and H. Isobe, *Angew. Chem., Int. Ed.*, 2022, **61**, e202204035.
21 Y. Segawa, M. Kuwayama, Y. Hijikata, M. Fushimi, T. Nishihara, J. Pirillo, J. Shirasaki, N. Kubota and K. Itami, *Science*, 2019, **365**, 272–276.
22 W. E. Barth and R. G. Lawton, *J. Am. Chem. Soc.*, 1971, **93**, 1730–1745.
23 M. M. Hashemi, M. S. Bratcher and L. T. Scott, *J. Am. Chem. Soc.*, 1992, **114**, 1920–1921.
24 L. T. Scott, M. M. Hashemi, D. T. Meyer and H. B. Warren, *J. Am. Chem. Soc.*, 1991, **113**, 7082–7084.
25 E. Nestoros and M. C. Stuparu, *Chem. Commun.*, 2018, **54**, 6503–6519.
26 L. T. Scott, P. C. Cheng, M. M. Hashemi, M. S. Bratcher, D. T. Meyer and H. B. Warren, *J. Am. Chem. Soc.*, 1997, **119**, 10963–10968.
27 H. Sakurai, T. Daiko and T. Hirao, *Science*, 2003, **301**, 1878.
28 S. Higashibayashi and H. Sakurai, *Chem. Lett.*, 2011, **40**, 122–128.
29 R. B. M. Ansems and L. T. Scott, *J. Am. Chem. Soc.*, 2000, **122**, 2719–2724.
30 K. Kawasumi, Q. Zhang, Y. Segawa, L. T. Scott and K. Itami, *Nat. Chem.*, 2013, **5**, 739–744.
31 K. Shoyama and F. Würthner, *J. Am. Chem. Soc.*, 2019, **141**, 13008–13012.

32 Z.-Z. Zhu, Z.-C. Chen, Y.-R. Yao, C.-H. Cui, S.-H. Li, X.-J. Zhao, Q. Zhang, H.-R. Tian, P.-Y. Xu, F.-F. Xie, X.-M. Xie, Y.-Z. Tan, S.-L. Deng, J. M. Quimby, L. T. Scott, S.-Y. Xie, R.-B. Huang and L.-S. Zheng, *Sci. Adv.*, 2019, **5**, eaaw0982.
33 Chaolumen, I. A. Stepek, K. E. Yamada, H. Ito and K. Itami, *Angew. Chem., Int. Ed.*, 2021, **60**, 23508–23532.
34 G. González Miera, S. Matsubara, H. Kono, K. Murakami and K. Itami, *Chem. Sci.*, 2022, **13**, 1848–1868.
35 S. H. Pun and Q. Miao, *Acc. Chem. Res.*, 2018, **51**, 1630–1642.
36 K. Y. Cheung, X. Xu and Q. Miao, *J. Am. Chem. Soc.*, 2015, **137**, 3910–3914.
37 K. Y. Cheung, C. K. Chan, Z. Liu and Q. Miao, *Angew. Chem.*, 2017, **56**, 9003–9007.
38 I. R. Márquez, S. Castro-Fernández, A. Millán and A. G. Campaña, *Chem. Commun.*, 2018, **54**, 6705–6718.
39 S. H. Pun, C. K. Chan, J. Luo, Z. Liu and Q. Miao, *Angew. Chem., Int. Ed.*, 2018, **57**, 1581–1586.
40 M. Randić, *Chem. Rev.*, 2003, **103**, 3449–3605.
41 M. A. Dobrowolski, A. Ciesielski and M. K. Cyrański, *Phys. Chem. Chem. Phys.*, 2011, **13**, 20557–20563.
42 O. El Bakouri, D. W. Szczepanik, K. Jorner, R. Ayub, P. Bultinck, M. Solà and H. Ottosson, *J. Am. Chem. Soc.*, 2022, **144**, 8560–8575.
43 Bharat, R. Bhola, T. Bally, A. Valente, M. K. Cyrański, Ł. Dobrzycki, S. M. Spain, P. Rempała, M. R. Chin and B. T. King, *Angew. Chem., Int. Ed.*, 2010, **49**, 399–402.
44 Y. Tanaka, N. Fukui and H. Shinokubo, *Nat. Commun.*, 2020, **11**, 3873.
45 C. Liu, Y. Ni, X. Lu, G. Li and J. Wu, *Acc. Chem. Res.*, 2019, **52**, 2309–2321.
46 J. C. Buttrick and B. T. King, *Chem. Soc. Rev.*, 2017, **46**, 7–20.
47 M. F. L. De Volder, S. H. Tawfick, R. H. Baughman and A. J. Hart, *Science*, 2013, **339**, 535–539.
48 W.-S. Wong and M. Stępień, *Trends Chem.*, 2022, **7**, 573–576.
49 M. Stępień, E. Gońka, M. Żyła and N. Sprutta, *Chem. Rev.*, 2017, **117**, 3479–3716.
50 A. Borissov, Y. K. Maurya, L. Moshniaha, W.-S. Wong, M. Żyła-Karwowska and M. Stępień, *Chem. Rev.*, 2022, **122**, 565–788.
51 (*a*) Q. Tan, S. Higashibayashi, S. Karanjit and H. Sakurai, *Nat. Commun.*, 2012, **3**, 10–15; (*b*) S. K. Pedersen, K. Eriksen and M. Pittelkow, *Angew. Chem., Int. Ed.*, 2019, **58**, 18419.
52 (*a*) C. G. Claessens, D. González-Rodríguez and T. Torres, *Chem. Rev.*, 2002, **102**, 835–854; (*b*) D. Myśliwiec, M. Stępień and M. St□pień, *Angew. Chem., Int. Ed.*, 2013, **52**, 1713–1717.
53 S. Ito, Y. Tokimaru and K. Nozaki, *Angew. Chem., Int. Ed.*, 2015, **54**, 7256–7260.
54 H. Yokoi, Y. Hiraoka, S. Hiroto, D. Sakamaki, S. Seki and H. Shinokubo, *Nat. Commun.*, 2015, **6**, 8215.
55 S. Higashibayashi, P. Pandit, R. Haruki, S. I. Adachi and R. Kumai, *Angew. Chem., Int. Ed.*, 2016, **55**, 10830–10834.
56 J. Wagner, P. Zimmermann Crocomo, M. A. Kochman, A. Kubas, P. Data and M. Lindner, *Angew. Chem., Int. Ed.*, 2022, **61**, e202202232.
57 K. Oki, M. Takase, S. Mori, A. Shiotari, Y. Sugimoto, K. Ohara, T. Okujima and H. Uno, *J. Am. Chem. Soc.*, 2018, **140**, 10430–10434.
58 T. Kirschbaum, F. Rominger and M. Mastalerz, *Chem.–Eur. J.*, 2020, **26**, 14560–14564.
59 P. An, R. Li, B. Ma, R. He, Y. Zhang, M. Xiao and B. Zhang, *Angew. Chem., Int. Ed.*, 2021, **60**, 24478–24483.
60 Z. Qiu, X. Chen, Y. Huang, R. Wei, K. Chu, X. Zhao and Y. Tan, *Angew. Chem., Int. Ed.*, 2022, **61**, e202116955.
61 (*a*) M. Krzeszewski, D. Gryko and D. T. Gryko, *Acc. Chem. Res.*, 2017, **50**, 2334–2345; (*b*) G. Sanil, B. Koszarna, Y. M. Poronik, O. Vakuliuk, B. Szymański, D. Kusy and D. T. Gryko, The Chemistry of 1,4-Dihydropyrrolo[3,2-b] pyrroles, *Adv. Heterocyclic Chem.*, 2022, **138**, 335–409.
62 F. Banhart, J. Kotakoski and A. V. Krasheninnikov, *ACS Nano*, 2011, **5**, 26–41.
63 T. Xu and L. Sun, in *Defects in Advanced Electronic Materials and Novel Low Dimensional Structures*, Elsevier, 2018, pp. 137–160.
64 Y. Fei, Y. Fu, X. Bai, L. Du, Z. Li, H. Komber, K. H. Low, S. Zhou, D. L. Phillips, X. Feng and J. Liu, *J. Am. Chem. Soc.*, 2021, **143**, 2353–2360.
65 S. Mishra, M. Krzeszewski, C. A. Pignedoli, P. Ruffieux, R. Fasel and D. T. Gryko, *Nat. Commun.*, 2018, **9**, 1714.
66 M. Krzeszewski, Ł. Dobrzycki, A. L. Sobolewski, M. K. Cyrański and D. T. Gryko, *Angew. Chem., Int. Ed.*, 2021, **60**, 14998–15005.
67 M. Grzybowski, K. Skonieczny, H. Butenschön and D. T. Gryko, *Angew. Chem., Int. Ed.*, 2013, **52**, 9900–9930.
68 M. Grzybowski, B. Sadowski, H. Butenschön and D. T. Gryko, *Angew. Chem., Int. Ed.*, 2020, **59**, 2998–3027.
69 P. Rempala, J. Kroulík and B. T. King, *J. Am. Chem. Soc.*, 2004, **126**, 15002–15003.
70 Y. Zhang, S. H. Pun and Q. Miao, *Chem. Rev.*, 2022, **122**, 14554–14593.
71 W. Hagui, H. Doucet and J.-F. Soulé, *Chem*, 2019, **5**, 2006–2078.
72 M. Tasior, O. Vakuliuk, D. Koga, B. Koszarna, K. Górski, M. Grzybowski, Ł. Kielesiński, M. Krzeszewski and D. T. Gryko, *J. Org. Chem.*, 2020, **85**, 13529–13543.
73 M. Krzeszewski, K. Sahara, Y. M. Poronik, T. Kubo and D. T. Gryko, *Org. Lett.*, 2018, **20**, 1517–1520.
74 J. Liu, A. Narita, S. Osella, W. Zhang, D. Schollmeyer, D. Beljonne, X. Feng and K. Müllen, *J. Am. Chem. Soc.*, 2016, **138**, 2602–2608.
75 J. P. Lewtak, D. Gryko, D. Bao, E. Sebai, O. Vakuliuk, M. Ścigaj and D. T. Gryko, *Org. Biomol. Chem.*, 2011, **9**, 8178–8181.
76 R. L. Martin, *J. Chem. Phys.*, 2003, **118**, 4775–4777.
77 A. Janiga, M. Krzeszewski and D. T. Gryko, *Chem.–Asian J.*, 2015, **10**, 212–218.